Mon. Not. R. Astron. Soc. **000**, 000–000 (2001)

Mirror eclipses in the cataclysmic variable IP Peg

S. P. Littlefair,[1] V. S. Dhillon,[1] T. R. Marsh[2] and E. T. Harlaftis[3]
[1] *Department of Physics and Astronomy, University of Sheffield, Sheffield S3 7RH, UK*
[2] *Department of Physics and Astronomy, University of Southampton, Highfield, Southampton SO17 1BJ, UK*
[3] *Institute of Astronomy and Astrophysics, National Observatory of Athens, P.O. Box 20048, Athens 11810, Greece*

Accepted for publication in the Monthly Notices of the Royal Astronomical Society

8 June 2001

ABSTRACT
We present time resolved K-band infrared spectra of the dwarf nova (DN) IP Peg in early quiescence. The Brackett-γ and He-I (λ2.0581) lines in our data shows hitherto unseen behaviour, which we term a *mirror eclipse*, and interpret as an eclipse of the secondary star by an optically thin accretion disc. Mirror eclipses are a direct probe of the structure and physical conditions of accretion discs. For example, on assuming the relevant level populations to be in LTE, we constrain the temperature and density of the optically thin material causing the mirror eclipse in IP Peg to be $10,000 \lesssim T \lesssim 20,000$K and $\rho \sim 10^{-11}$g cm^{-3} respectively. In order to match our data, we find that at least the outermost 20% of the disc (in radius) must be entirely optically thin. Implications for time-dependent disc models are examined.

Key words: binaries: close – stars: individual: IP Peg – dwarf novae, accretion, cataclysmic variables – infrared: stars

1 INTRODUCTION

Cataclysmic variables (CVs) are semi-detached binary systems in which a white dwarf primary star accretes material from a Roche-lobe filling secondary star via an accretion disc or a magnetically-channelled accretion flow. For a thorough review of CVs, see **?**.

Dwarf novae (DNe) form a sub-class of the non-magnetic CVs, which are characterised by their quasi-periodic outbursts with amplitudes between 2 and 6 magnitudes and intervals ranging from days to many years. These outbursts are generally held to be caused by an instability within the accretion disc – an idea first advanced by **?** and later developed by **?** and **?**. The disc instability hypothesis (and the models based upon it) has had considerable success in describing the characteristics of dwarf novae outbursts, with the amplitudes, periodicities, spectral evolution and basic shapes of observed outbursts being well-reproduced by the models (**?**).

However, it has long been suspected that the discs in dwarf novae at quiescence are quite unlike those predicted by the thermal-viscous disc instability model (DIM). For physically viable values of the disc viscosity parameter, α, the models produce discs which are optically thick. Evidence exists, however, which suggests that the discs in some dwarf novae are optically thin - eclipse mapping of quiescent DN accretion discs give disc colours which are strongly suggestive of optically thin gas (e.g. **?**, **?**). Also, white dwarf eclipse light curves suggest an optically thin disc (**?**). Furthermore, all versions of the DIM predict increasing fluxes from the disc during quiescence, whilst observations show that these fluxes stay constant or decrease. In a recent review, **?** calls dwarf novae in quiescence the "Achille's heel" of the DIM.

In this paper we present time-resolved K-band spectra of the dwarf nova IP Peg. IP Peg is a deeply eclipsing system with a period of ∼3.8 hrs. It is the brightest eclipsing dwarf nova above the period gap and, as such, is a well-studied and important system. The Brackett-γ and He-I (λ2.0581) lines in our data show hitherto unseen behaviour – a reduction in equivalent width, centred on binary phase 0.5, which appears in the trailed spectra as a mirror-image of the classical rotational disturbance, or *Z-wave* (**?**).

We argue that this feature results from an eclipse of the secondary star by an optically thin accretion disc. We model the effect in order to determine: i) whether the optically thin region forms the main part of the disc, and ii) the temperature and density of the optically thin regions.

2 OBSERVATIONS

On the night of 1998 August 10 and again on the nights of 2000 June 18,19 and 20 we obtained spectra of the dwarf nova IP Peg and the M4-dwarf Gl402 with the Cooled Grating Spectrometer 4 (CGS4) on the 3.8 m United Kingdom Infrared Telescope (UKIRT) on Mauna Kea, Hawaii. Both observation periods corresponded to early quiescence, 17-20 days after decline from outburst. CGS4 is a 1–5 micron spectrometer containing an InSb array with 256×256 pixels. The 40 l/mm grating with the 300 mm camera gave a resolution of approximately 350 $\mathrm{km\,s^{-1}}$. To cover the wavelength range 1.81–2.51 microns required one grating setting, centred at 2.124 microns (first order). Optimum spectral sampling and bad pixel removal were obtained by mechanically shifting the array over two pixels in the dispersion direction in steps of 0.5 pixels. We employed the non-destructive readout mode of the detector to reduce the readout noise. In order to compensate for fluctuating atmospheric OH^- emission lines we took relatively short exposures (typically 30 seconds) and nodded the telescope primary so that the object spectrum switched between two different spatial positions on the detector. The slit width was 0.6 arcseconds (projecting to approximately 1 pixel on the detector) and was oriented at the parallactic angle. On the first run, conditions were excellent. Using the UKIRT tip-tilt secondary, the seeing was around $0.5''$. The humidity was low (10-20%) throughout, and the sky was photometric for the duration of the run. The second run also had good conditions, with seeing usually around $0.5''$ and photometric skies. Unfortunately, a full computer disc interrupted observations near phase 0.5 on the first night.

A full journal of observations is presented in table 1.

3 DATA REDUCTION

The initial steps in the reduction of the 2D frames were performed automatically by the CGS4 data reduction system (**?**). These were: the application of the bad pixel mask, bias and dark frame subtraction, flat field division, interlacing integrations taken at different detector positions, and co-adding and subtracting nodded frames. Further details of the above procedures may be found in the review by **?**. In order to obtain 1D data, we removed the residual sky by subtracting a polynomial fit and then extracted the spectra using an optimal extraction technique (**?**). The next step was the removal of the ripple arising from variations in the star brightness between integrations (i.e. at different detector positions). These variations were due to changes in the seeing, sky transparency and the slight motion of the stellar image relative to the slit.

There were two stages to the calibration of the spectra. The first was the calibration of the wavelength scale using krypton arc-lamp exposures. A fourth-order polynomial fit to the arc lines yielded an error of less than 0.0001 microns (rms) and the error in the fit showed no systematic trend with wavelength. The final step in the spectral calibration was the removal of telluric features and flux calibration. This was performed by dividing the spectra to be calibrated by the spectrum of an F-type standard star, with its prominent stellar features interpolated across. F-type stars were taken throughout the night, at different airmasses. In each case, the F-type star used was that which gave the best removal of telluric features, which was judged by inspection of the residuals. We then multiplied the result by the known flux of the standard at each wavelength, determined using a black body function set to the same effective temperature and flux as the standard. As well as correcting for the spectral response of the detector, this procedure also removed telluric absorption features from the object spectra. No correction for slit losses was made and the absolute flux in each spectrum is hence unreliable.

4 RESULTS

4.1 Average spectra and secondary star contribution

Figure 1 shows the average spectra of IP Peg from the first run, both in our rest frame and in the rest frame of the secondary star. The spectra of IP Peg in our rest frame (top) shows that the emission line of Brackett-γ exhibits the double peaked line profile characteristic of high-inclination accretion discs. The central and lower spectra show that the M4-dwarf secondary star (**?**) dominates the K-band light in IP Peg. In order to calculate the contribution of the secondary star to the K-band light, the spectra of both IP Peg and Gl402 were normalised and a spline fit to the continuum was subtracted. The spectrum of Gl402 was multiplied by a constant and subtracted from the spectrum of IP Peg. This constant was then adjusted to minimise the scatter between the residual spectrum and a smoothed version of the residual spectrum. We found that the secondary star in IP Peg contributes $62 \pm 3\%$ of the K-band light.

4.2 Time resolved spectra

Figure 2 shows the time-resolved spectra of IP Peg in a trailed format. The data were phased according to the ephemeris of **?**, derived from the TiO radial velocity curves of the secondary star; the radial velocity curves of the secondary star absorption lines in our data were found to be consistent with this ephemeris.

Considering the first run (left hand panel), two "eclipses" are seen in the data, a primary eclipse centred on phase 0.0 (when the secondary star lies between the disc and the Earth) and a secondary "eclipse" centred on phase 0.5 and seen again after one orbital cycle at phase 1.5. The primary eclipse is due to the obscuration of light from the disc by the opaque secondary star. This eclipse is characterised by the initial eclipse of blue-shifted disc emission, as the secondary star first occults material from the disc which is moving towards the Earth. Later in the eclipse the receding, red-shifted part of the disc is obscured. This is the classic rotational disturbance pattern.

It is the secondary "eclipse" which is remarkable. At these phases it is the red-shifted, receding half of the emission line that is affected first. The feature possesses a telling mirror-symmetry with the classical rotational disturbance seen in the primary eclipse. It is this feature which has led us to term this a *mirror eclipse*.

The mirror eclipse can be understood as follows. If the

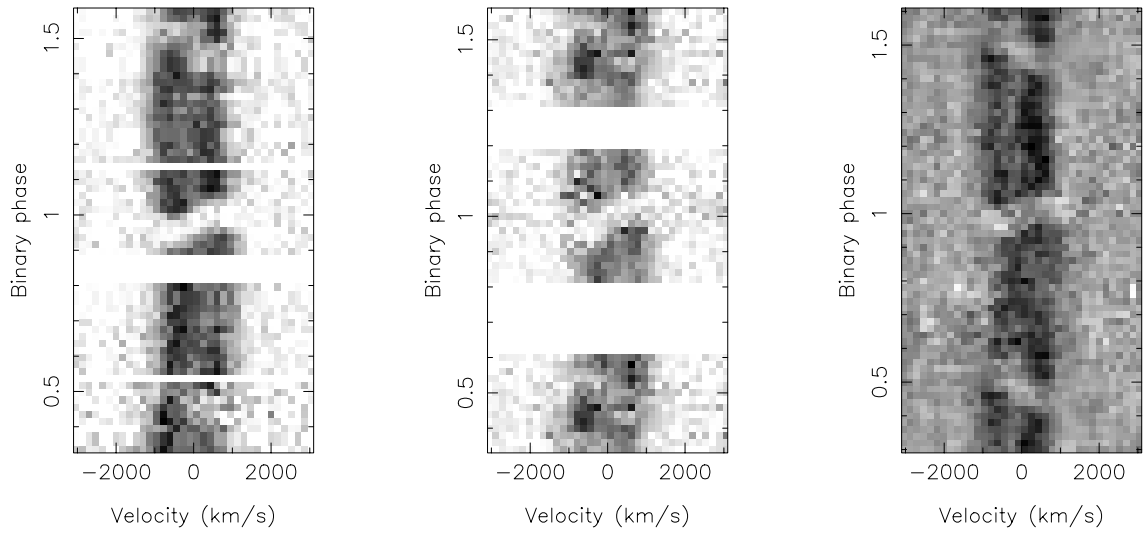

Figure 2. Time-resolved K-Band spectra of the dwarf nova IP Peg. Dark pixels represent strong emission. The individual spectra have been normalised by fitting a constant to the continuum and dividing by this fit, and a spline fit to the continuum has been subtracted. Gaps show periods where observations of IP Peg were interrupted to observe a calibration star. The left hand panel shows the Brackett-γ line from the first run, taken on 1998 August 10. The middle panel shows the Brackett-γ line from the second set of data, taken on the nights of 2000 June 18,19,20. The spectra in this panel have been phase binned to improve signal-to-noise. The right-hand panel shows the He-I (λ2.0581) line, where the data from all runs has been averaged into fifty phase bins. The middle and right-hand panels have been phase folded to cover the same range of phases as the left-hand panel.

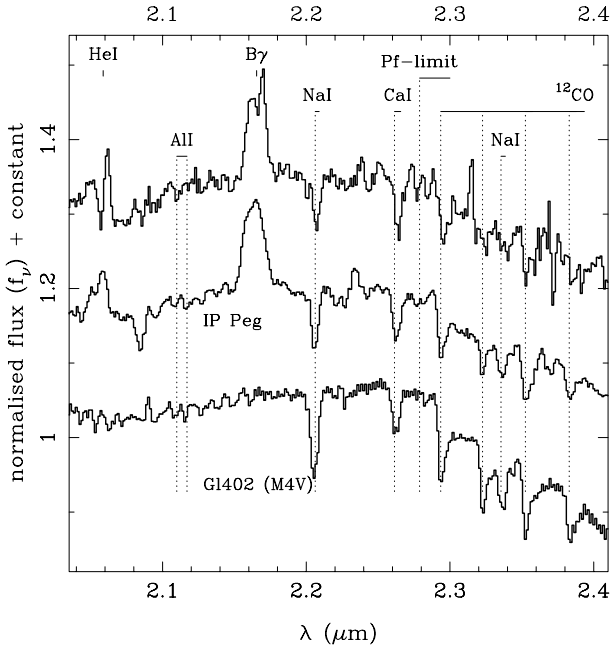

Figure 1. Average K-band spectra from the first run of the dwarf nova IP Peg and the average spectrum of the M4-dwarf Gl402. The upper spectrum is the straight average of the time-resolved spectra of IP Peg. The middle spectrum is an average of the same spectra in the rest frame of the secondary star; i.e. before averaging, the time-resolved spectra of IP Peg were shifted in wavelength to correct for the radial velocity of the secondary star. Each spectrum has been normalised by dividing by the flux at 2.3 μm and offset by a multiple of 0.15.

disc were not wholly opaque, but optically thin we would see an unusual effect. For a strong line, the absorption coefficient must be higher at emission line wavelengths than in the continuum. Hence, more of the secondary star light is absorbed by the disc at wavelengths corresponding to the emission lines. Superimposing the contributions from disc and secondary star, the absorption of secondary star light by the disc reduces the total amount of light at wavelengths corresponding to the emission lines. As the part of the disc which initially occults the secondary star is moving away from us, we first see the red-shifted gas affected. During the later stages of the eclipse, the red-shifted emission is unaffected whilst the blue-shifted gas is now responsible for the absorption. This is exactly the behaviour seen during the mirror eclipse. Thus, a mirror eclipse is nothing more than the eclipse of the secondary star by an optically thin disc.

The second run (figure 2 – middle panel) also shows the mirror eclipse, demonstrating that the effect is persistent over long timescales ($\sim$ 2 years). A mirror eclipse is also visible in the trailed spectrum of He-I (λ2.0581) (figure 2 - right hand panel.

It is not surprising that mirror eclipses have never been observed before, as this is the first time-resolved infrared spectroscopic study of an eclipsing CV with a bright secondary star; the amount of secondary star light absorbed is proportional to the intensity of the secondary star, hence mirror eclipses are not observed in optical spectra as the secondary stars are much fainter (both absolutely and relative to the accretion disc) at optical compared to infrared wavelengths.

5 MODELLING

Modelling of the mirror eclipse was undertaken with three aims in mind. First, we wanted to confirm that our hypothesis of an eclipse of the secondary star by an optically thin disc could satisfactorily reproduce the mirror eclipse as seen in the data. Second, it is possible that the mirror eclipse effect could also be caused by a geometrically thick, optically thin region overlying an optically thick disc. Just such a "sandwich-structure" has often been proposed to explain the formation of strong emission lines from optically thick discs (**?**). We wished to determine if our data were compatible with such a picture. Third, we wanted to determine, if possible, the temperature and density of the gas causing the mirror eclipse.

Because our data contains no reliable flux information the data were first normalised by fitting a constant to the continuum, then dividing the spectra by this fit. Finally, a spline fit to the continuum around the line was subtracted to produce a continuum-subtracted trailed spectrum. In order to simplify modelling, we removed the radial velocity of the white dwarf from the trailed spectra, and averaged the spectra which were unaffected by either the primary or mirror eclipse. This average spectrum was then subtracted from the original trailed spectrum. The resulting profiles, with the disc emission removed, represent the absorption of the secondary star continuum by the accretion disc.

These absorption profiles were modelled as the absorption of secondary star light by a non-emitting, uniform disc. The disc in our model is uniform in both temperature and density, the continuum opacity is calculated according to the formulations in **?**. Contributions to the continuum opacity from H bound-free, H free-free, He-I free-free, He-I bound-free, He^- free-free and H^- were considered. Line opacities are calculated from the line lists of **?**. Stark broadening is included for the hydrogen lines using the tables of **?**. All opacities are calculated assuming LTE and solar abundances. The velocity field of the disc is assumed to be Keplerian and vertically uniform. We take a uniform intensity distribution on the secondary star and trace individual rays through the disc, solving the radiative transfer equation to calculate the emergent line profile from a single element of the secondary star. The line profiles from each element are then combined, and the resultant trailed spectrum is normalised and continuum subtracted in an identical fashion to the data. An estimate of the strength of the mirror eclipse is obtained from both data and model by calculating the average depth within a pre-defined region of the trailed spectra. It is necessary to input the system parameters of IP Peg into the code (masses, period and inclination). Allowing these values to vary within the range of values found in the literature did not significantly affect the results of modelling (see **?** for a discussion of possible system parameters for IP Peg). The results are shown in figure 3.

We see that our simple LTE model reproduces the mirror eclipse extremely well. Only the disc radius, disc height, density and temperature have been varied to achieve agreement. The disc radius used strongly affects both the strength and the overall shape of the eclipse. In particular it is the disc radius which determines the velocity of the minima of the absorption profiles. Disc radii of $0.5-0.7L_1$ were consistent with the data – we used a disc radius of $0.6L_1$, which corresponds to the disc radius found by eclipse mapping of the infrared (H-band) continuum by **?**. The disc height used was $0.06L_1$, corresponding to a disc opening angle of 6°. The quiescent disc height in IP Peg is unconstrained by observations; values for the opening angle in outburst vary from $\sim 10-20^\circ$ (**?**, **?**) and disc models predict quiescent opening angles of $\sim 4^\circ$ (**?**). Note that there is a strong correlation between the strength of the mirror eclipse and the disc height - increasing the disc height to $0.08L_1$ gave a 10 % increase in mirror eclipse strength.

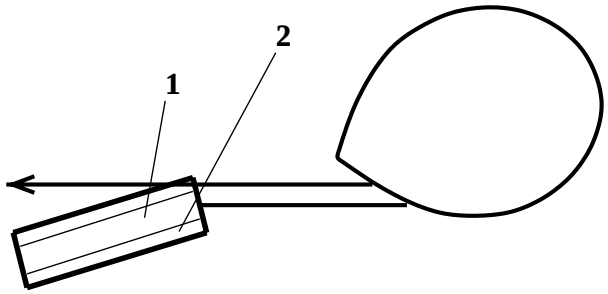

Figure 4. Diagram showing how the line wings constrain geometry of the disc.

The model satisfactorily reproduces the strength, timing and overall morphology of the mirror eclipse. Hence, we are confident that our interpretation of the effect is correct.

5.1 Disc structure (1) – The line wings

There has always been a difficulty reconciling the optically thick discs favored by models with the presence of strong emission lines which share the disc velocities. To overcome this, a chromosphere model has often been suggested, in which the disc is overlaid by an optically thin chromosphere which is the source of the emission lines, e.g. **?**. Further, **?** showed that the formation of a vertically extended corona is likely above a standard model disc. Both of these models propose a "sandwich structure" where optically thin material overlays a central, optically thick region.

We might constrain such a sandwich structure by looking at the line wings during mirror eclipse. The line wings originate from gas with high velocities, i.e. the inner disc. For the mirror eclipse effect to be present in the line wings requires that light from the secondary star can follow paths which both pass through the inner disc regions and do not intersect any optically thick regions of gas. An optically thick central plane would intercept rays passing through the inner disc. This is illustrated in figure 4. The disc is split into two regions. Region 1 is optically thick, and represents a "standard" model disc, region 2 is optically thin, and represents a chromosphere or vertically extended corona. Shown on the figure are two ray-paths from the secondary star to the observer. The lower ray, which passes through the inner disc, is absorbed by the optically thick central plane. The upper ray passes through the optically thin material at larger radii. Hence, in this situation a mirror eclipse would still be present in the line core (albeit at a lower intensity than if the disc were entirely optically thin), but there would be no mirror eclipse in the line wings. Unfortunately, there is insufficient signal-to-noise in our data to determine if the line

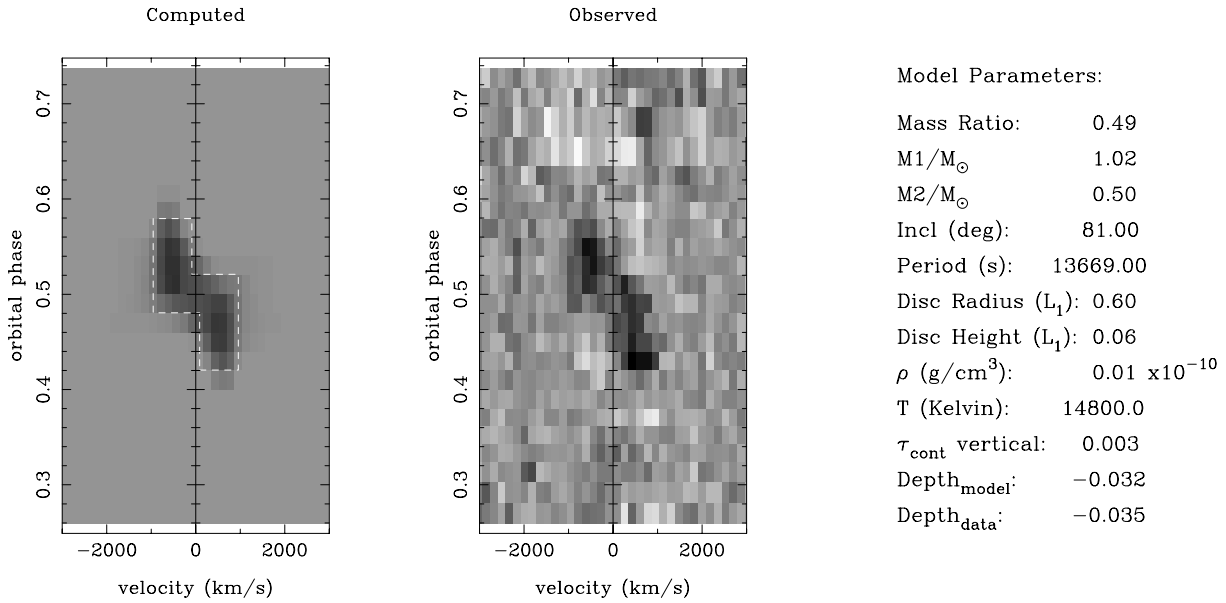

Figure 3. Results from the model described in section 5. Left: the computed spectra. The region used to calculate the strength of the mirror eclipse is shown with a dotted line. Right: the observed spectra, plotted on the same greyscale as the left-hand panel. The dataset shown is the mirror eclipse of the Brackett-γ line. Spectra from all the runs have been averaged into fifty phase bins. The parameters used in the model are representative values for IP Peg (table 2 in **?**). The disc radius and height are quoted in units of distance to the inner Lagrangian point. In both panels, dark pixels represent strong absorption.

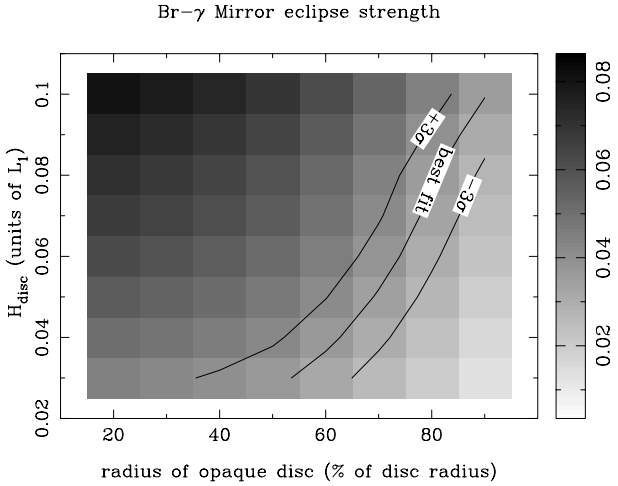

Figure 5. Plot of Brackett-γ mirror eclipse strength as a function of disc height and radius of an opaque obstruction located in the disc midplane. Mirror eclipse strength is calulated as described in section 5, paragraph 3. It is a dimensionless quantity. Calculations are for a disc radius of $0.6L_1$, temperature of $6800K$ and a density of 1.12×10^{-11} g cm^{-3}. Contour lines of constant mirror eclipse strength are plotted at the strength of the Brackett-γ eclipse in the data, and at the 3σ levels.

wings participate in the mirror eclipses exhibited by IP Peg. We can, however, obtain weaker constraints on the structure of the disc by looking at the whole line

5.2 Disc structure (2) – Constraints on an optically thick midplane

Figure 5 shows the effect of a sandwich-structured disc on the strength of the Brackett-γ mirror eclipse. Using the code outlined in section 5, we added an infinitely thin, optically thick central plane. The emergent spectrum of any ray which intersected this plane was set to zero. Figure 5 shows the depth of the mirror eclipse as a function of accretion disc height and the radius of the optically thick plane. In order to determine strict upper limits on the size of an optically thick, central plane we used a temperature of 6800K and a density of 1.12×10^{-11} g cm^{-3}. These parameters give the strongest mirror eclipse effect and so would allow the largest possible central obstruction. The -3σ contour plotted shows the minimum strength of mirror eclipse which is consistent with our data. Models to the right of this line cannot be reconciled with the observations. For a disc height of $0.06L_1$ this suggests that an infinitely thin, optically thick midplane must have a radius of less than $\sim$ 80% of the disc radius. The +3σ contour seems to suggest that part of the disc must be opaque in order to fit the strength of the mirror eclipse in the data. This is not the case, however, as we have used the temperature and density which give the strongest mirror eclipse effect. Temperatures and densities which produce weaker mirror eclipse effects would allow a disc which is wholly optically thin.

This result places strong limits on the extent of a sandwich structure for the disc in IP Peg. Even if we use those temperatures and densities which permit the largest possible optically thick midplane and restrict the midplane itself to be infinitely thin, we still find that the outermost 20% of the disc (in radius) must be entirely optically thin.

Note that a larger opaque central plane is permitted by invoking a thicker overall disc (e. g. a disc height of $0.08L_1$

allows an optically thick midplane with a radius of $\sim 90\%$ of the disc radius, and a disc height of $0.1L_1$ allows an optically thick midplane with a radius of 100% of the disc radius). The disc opening angle in IP Peg in outburst varies from $\sim 10 - 20^\circ$ (**?**, **?**), corresponding to an outurst disc height of $0.01 - 0.02L_1$. It is therefore unlikely that the quiescent disc is as thick as $0.01L_1$. Other possibilities which allow a thicker disc are a vertically extended chromosphere or corona. It is unlikely that coronal gas could be responsible for the mirror eclipse (see section 5.3), but a vertically extended chromosphere remains a possibility.

5.3 Physical conditions of the optically thin gas

The presence of the mirror eclipse gives constraints on the density and temperature of the gas within the disc. This is because the mirror eclipse requires both an optically thin continuum and a significant line opacity. Figure 6 shows how the continuum opacity and Brackett-γ opacities vary with density and temperature. Also shown is the strength of the mirror eclipse effect over the same parameter space. *Note that no optically thick midplane was used when calculating this strength.* Considering the variation in the opacities with temperature (top-left panel), it is seen that a sharp onset of the mirror eclipse effect is to be expected at the temperature where the Brackett-γ opacity suddenly increases. Below this temperature, although the disc is optically thin, there is no significant Brackett-γ opacity and a mirror eclipse cannot occur. As the temperature increases further, the continuum opacity rises quickly and the condition that the disc is optically thin in the continuum is no longer satisfied. We therefore expect the mirror eclipse effect to be concentrated in the area close to the sudden rise of the line opacity. Extending our parameter space to include variations in density, we see that the continuum opacity increases strongly towards higher temperatures and densities (bottom-left panel), whilst the Brackett-γ opacity increases rapidly with respect to the continuum opacity along bow-shaped fronts (top-right panel). By comparison with the earlier example, we would therefore expect the mirror eclipse to be concentrated along these fronts, weakening towards higher temperatures and densities, which is exactly what the model shows (bottom-right panel).

Figure 7 shows the variation in continuum opacity, He-I (λ2.0581) line opacity and depth of mirror eclipse as a function of temperature and density. The mirror eclipse is confined to a relatively small region of parameter space (bottom-right hand panel). Combining this with the modelling of the Brackett-γ mirror eclipse and further assuming that the same regions of gas are responsible for the effect in both lines (which seems reasonable given the similarities between the two line profiles) we can obtain rather tight constraints on the temperature and density of the gas responsible for the mirror eclipse. This is shown in figure 8.

Using constraints on the strength of the Brackett-γ mirror eclipse in the data we can constrain the temperature and density of the gas causing the mirror eclipse to lie within the dashed contours shown in figure 8. These contours form a band in temperature-density space. Temperatures and densities inside the area bounded by this band produce a mirror eclipse which is too strong to fit the observed data; temperatures and densities outside the area bounded by the band produce too weak a mirror eclipse. Similarly, the strength of the mirror eclipse in He I constrains the temperatures and densities to be within the band defined by the solid contours in figure 8. The solid-shaded region in figure 8 therefore represents those temperatures and densities which are consistent with the strengths of the observed mirror eclipses in *both* Brackett-γ and He-I.

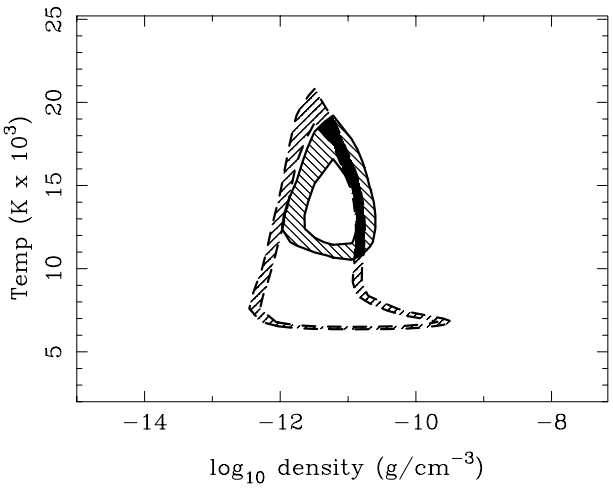

Figure 8. Regions of temperature-density space which are consistent with our data. The solid contour bounds the region of parameter space consistent with the strength of the mirror eclipse in the He-I (λ2.0581) line. The dashed line similarly represents temperatures and densities consistent with the strength of the mirror eclipse in the Brackett-γ line (the contour levels are determined by the strength of the mirror eclipse in the data, plus or minus 3σ). The solid region represents temperatures and densities which are consistent with the observations of mirror eclipses in both lines.

Our modelling of the conditions in the disc of IP Peg show that the gas responsible for the mirror eclipse has a temperature between 10,000 and 20,000 K and a density of $\sim 10^{-11}$ g cm^{-3} (assuming the relevant level populations are in LTE). Brightness temperatures for the quiescent disc in IP Peg have been derived by eclipse mapping in the optical and the infrared. Using H-band data, **?** find a brightness temperature of 3000 K, whilst **?** use optical data to find brightness temperatures between 4000 and 6500 K. Since these brightness temperatures represent lower limits to the effective temperature of the disc, they are not inconsistent with our findings.

These results are not easily reconciled with the DIM, where the *midplane* temperature may be as low as 2000 – 3000 K (**?**). Certainly the DIM predicts that the effective temperature in the disc must everywhere be below the critical value $T_{crit} \sim 5800$ K (**?**), nearly a factor of two lower than the temperatures which we find for the gas causing the mirror eclipse. It is possible, however, that the gas causing the mirror eclipse is found in an overlying chromosphere (but see section 5.2). It is also possible that the high temperatures observed in dwarf novae accretion discs in quiescence is a consequence of the disc being optically thin and hence radiatively inefficient. **?** found that optically thin discs pos-

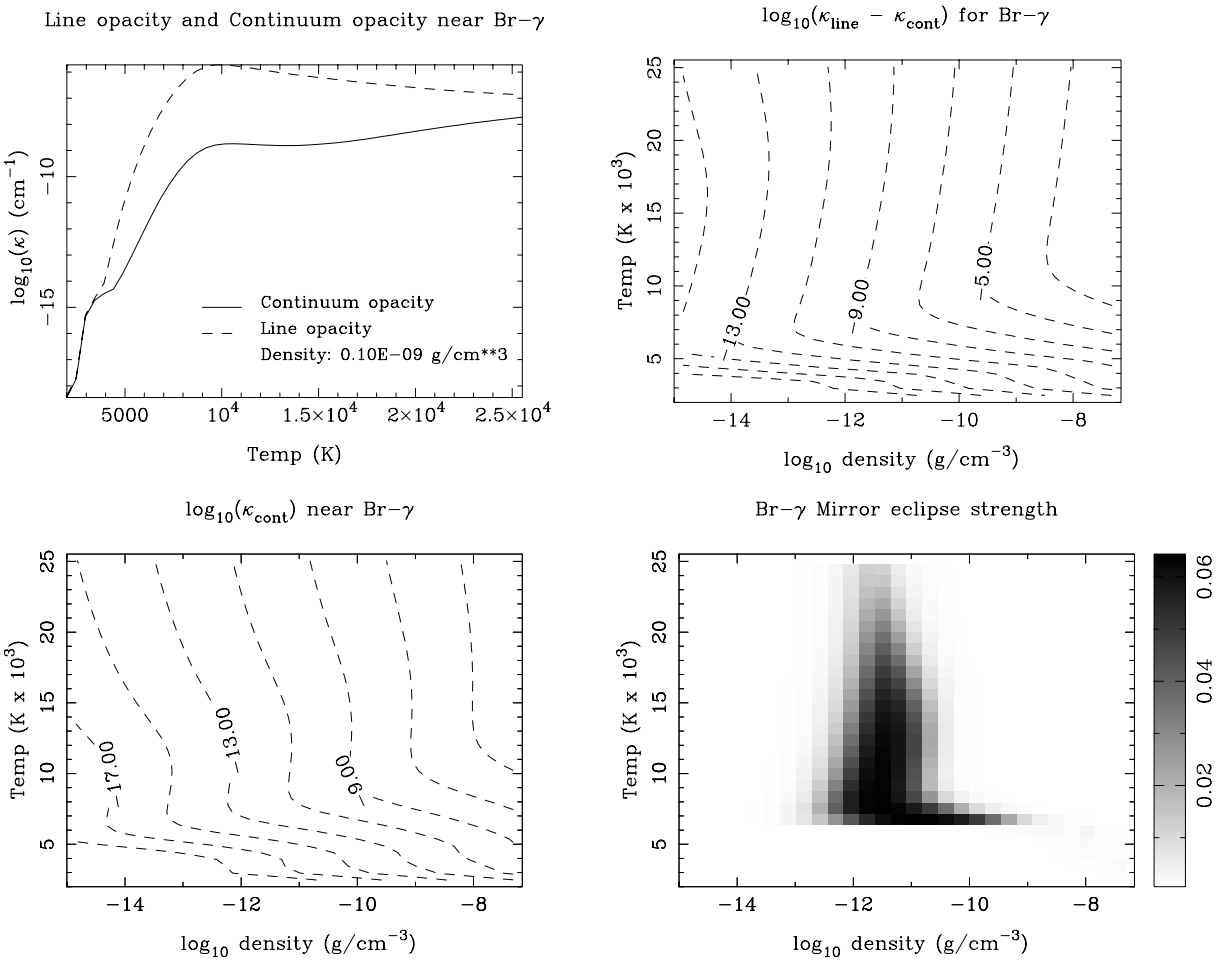

Figure 6. Top left: continuum and Brackett-γ line opacity versus temperature for a constant density. Bottom left: $\log_{10}$ continuum opacity as a function of temperature and density. Top right: $\log_{10}$ difference between line and continuum opacities as a function of density and temperature. Bottom right: strength of mirror eclipse in Brackett-γ line as a function of density and temperature. Mirror eclipse strength is calulated as described in section 5, paragraph 3. It is a dimensionless quantity. All models assume LTE and solar abundances.

sessed a "thermostat effect", their temperature never dropping below 6000 K.

The main conclusion we can draw about the midplane of the disc is that it must be optically thin in the K-band in its outer parts. It would be useful if future disc models could compute the K-band optical depth as a function of disc radius.

6 DISCUSSION

This is by no means the first evidence that the disc in IP Peg is optically thin at quiescence. **?** also found evidence for an optically thin disc from the size of the secondary eclipse in the H-band lightcurves, although their analysis required a complex and uncertain decomposition of the lightcurve. **?** studied the TiO band in IP Peg, and found a considerable reduction in band strength around phase 0.5. They required a very large (approximately the same size as the white dwarf's Roche Lobe), optically thick disc in order to match the strength of the band variations, in contrast to the study by **?**. We suggest that the difference between these studies could be reconciled if irradiation from the white dwarf concentrated the TiO absorption towards the outer hemisphere of the secondary star (e.g. **?**). Although **?** found no significant ellipticity in the radial velocity curves of TiO, this does not necessarily imply a uniform light distribution on the surface of the secondary star, merely that the light distribution is symmetric about the line of centres. Alternatively, if the TiO absorption on the secondary star was concentrated in star-spot regions, the large reduction in band strength seen by **?** could be caused by a relatively small optically thick region, i.e. the bright spot. Hence, we believe there is now an overwhelming body of evidence that the outer disc in IP Peg is optically thin in quiescence.

6.1 The future of mirror eclipses

Mirror eclipses have the potential to be an important tool in the study of accretion disc physics. The presence of mirror eclipses is sensitive to the detailed atomic physics which control line opacity. The detection of mirror eclipses in more lines will therefore allow us to determine even more precisely the physical conditions of the gas within the disc. Mirror

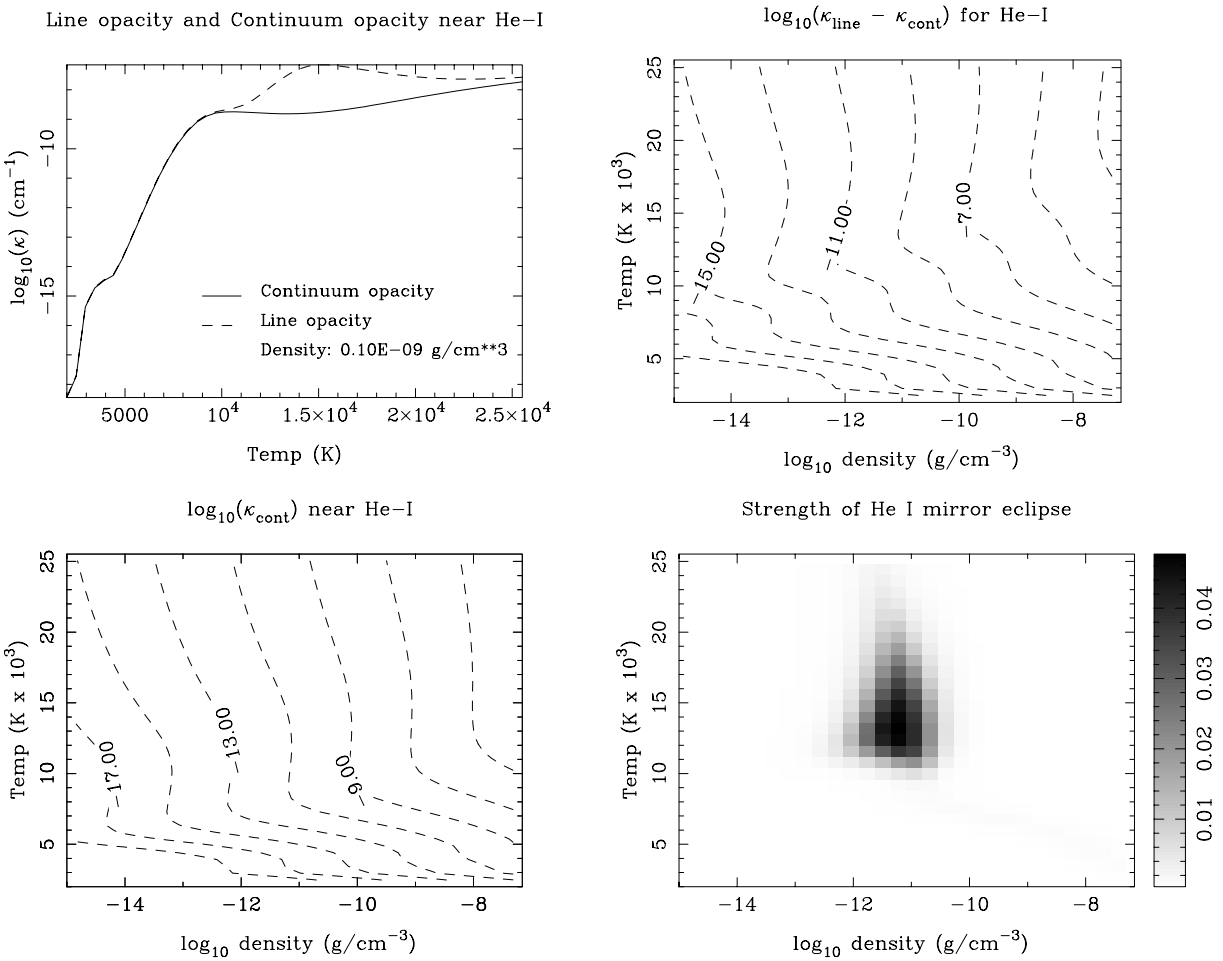

Figure 7. Top left: continuum and He I (λ2.0581) line opacity versus temperature for a constant density. Bottom left: $\log_{10}$ continuum opacity as a function of temperature and density. Top right: $\log_{10}$ difference between line and continuum opacities as a function of density and temperature. Bottom right: strength of mirror eclipse in He I (λ2.0581) line as a function of density and temperature. Mirror eclipse strength is calulated as described in section 5, paragraph 3. It is a dimensionless quantity. All models assume LTE and solar abundances.

eclipses may lend themselves to tomography, allowing maps of temperature and density within the disc to be made. Such extensions will require datasets of extremely high signal-to-noise. Future studies should also include a study of mirror eclipses throughout an outburst cycle, allowing a picture of how mass builds up in the disc to be formed.

7 CONCLUSIONS

A *mirror eclipse* is an eclipse of the secondary star by an optically thin accretion disc. The mirror eclipse appears in the trailed spectra as a reduction in equivalent width of the emission lines. The mirror eclipse is velocity-dependent, with the red-shifted part of the emission line being affected before the blue (as expected for the sense of the rotation of the disc and binary system). This leads to the mirror eclipse possesing a telling mirror-symmetry with the classical rotational disturbance pattern seen in the primary eclipse. The mirror eclipse is a consequence of a strong opacity within the line, combined with an optically thin continuum.

As such, the observation of the mirror eclipse in IP Peg provides clear evidence that at least the outer radial part of the accretion disc is optically thin. We find that an infintely thin opaque layer in the central plane of the disc cannot extend beyond about 80% of the disc radius and still be consistent with observations.

Standard disc instability models predict optically thick discs. Modifications to the standard disc instability models already exist which may be compatible with our data. Such a model has been described by **?**, in which the accreted material is stored in an optically thick torus between outbursts. If this torus were surrounded by optically thin gas this could be responsible for the observed mirror eclipses.

Because the mirror eclipse is a reasonably direct probe of the physical conditions within the disc, it provides an important diagnostic tool, allowing determinations of the temperature, density and structure of optically thin accretion discs. For example, assuming the relevant level populations are in LTE, we constrain the temperature and density of the optically thin material causing the mirror eclipse in IP Peg to be $10,000 \lesssim T \lesssim 20,000$K and $\rho \sim 10^{-11}\,\mathrm{g\,cm^{-3}}$ respectively.

Acknowledgements

SPL is supported by a PPARC studentship. ETH was partially supported for the UKIRT observing trip by the Hellenic Astronomical Society. UKIRT is operated by the Joint Astronomy Centre on behalf of the Particle Physics and Astronomy Research Council. The authors acknowledge the data analysis facilities at Sheffield provided by the Starlink Project which is run by CCLRC on behalf of PPARC. The authors would like to thank Rob Robinson and Tim Naylor for enlightening discussions and the referee and editor for their useful comments.

Table 1. Journal of observations. Each spectrum consists of 120 s total exposure time, excepting those marked[1], which consist of 80 s total exposure time. Gaps between objects were used for the observation of arcs, flats and F-star spectra. On 18/06/00 the spectra surrounding phase 0.5 were lost due to a disk crash. Orbital phase is shown for IP Peg using the ephemeris of **?**.

Object	Date	UT start	UT end	No. of Spectra	Phase start	Phase end
IP Peg	**10/08/98**	**09:54**	**13:12**	**78**	**0.23**	**1.08**
IP Peg	**10/08/98**	**13:17**	**14:55**	**24**	**1.12**	**1.53**
IP Peg	**18/06/00**	**11:50**	**13:27**	**36**	**0.26**	**0.67**
IP Peg	**18/06/00**	**13:44**	**14:40**	**24**	**0.76**	**0.99**
IP Peg	**18/06/00**	**14:42**	**15:10**	**12**	**1.01**	**1.12**
IP Peg	**19/06/00**	**14:30**	**14:38**	**4**	**0.28**	**0.31**
IP Peg[1]	**19/06/00**	**14:38**	**15:19**	**24**	**0.32**	**0.48**
IP Peg[1]	**20/06/00**	**14:01**	**14:19**	**12**	**0.47**	**0.55**